Optical Wireless Communication Conference

VCSEL Modeling for Optical Wireless Communications

Hao Bai[1], Songsui Li[1] Xiong Deng[1*]
[1]Center for Information Photonics and Communications,
Southwest Jiaotong University, Chengdu 611756,China.
[*] xiongdeng@swjtu.edu.cn

Abstract—The rate equations of vertical-cavity surface-emitting lasers (VCSELs) have been modelled incorporating the noise and thermal effect. The discrete-time model is simulated and compared with three numerical methods. It is further embedded into our self-developed simulation software and compared with other commercial ones. An accurate VCSEL channel model can facilitate the system design and inspire novel digital signal processing algorithms for optical wireless communications (OWC).

Index Terms — Rate equations, semiconductor lasers, vertical-cavity surface-emitting lasers, simulation software.

Ⅰ Introduction

Semiconductor laser is one of the most representative key optoelectronic devices, and has been widely used in many fields such as communications and display. Conventional edge-emitting lasers emit light in a direction parallel to the substrate, making it impossible to achieve face-to-face free-space optical interconnections, optical switching and parallel processing. It wasn't until the advent of the vertical-cavity surface emitting laser (VCSEL) that this changed. The VCSEL was invented by K. Iga of Tokyo Institute of Technology in 1979[1],[2]. Compared with edge-emitting semiconductor lasers, the VCSELs offer a variety of advantages[3]. The main advantages of the VCSELs are single-longitudinal-mode operation, circular output beams, suitability for monolithic 2-D integration, and direct modulation[4]-[6]. It is because of these advantages that VCSELs are widely used in high-speed optical communications, optical interconnects and other fields[8],[9].

Rate equations provide a powerful tool for laser design, optimization and performance analysis. Therefore, it is of interest for the study rate equations of VCSEL model. For example, P.V. Mena et al. presented a VCSEL model based on the standard laser rate equations by introducing a thermally dependent empirical offset current[10].

In this paper, we discuss the rate equations and the method of solving the equations using discrete-time approaches. We then simulate the LI characteristics and dynamic response of the VCSEL and compare them with references. In addition, a comparison is made with simulation softwares.

Ⅱ Models

A. Simple rate equations

The operating characteristics of a semiconductor laser can be described by a set of rate equations, which is a set of differential equations describing the interaction between photons and electrons in the active region of a semiconductor laser. The general form of the semiconductor laser's single-mode rate equations are as follows[11]

$$\begin{cases} \dfrac{dN}{dt} = \dfrac{\eta_i I}{q} - \dfrac{N}{\tau_n} - \dfrac{G_0(N-N_0)S}{1+\varepsilon S} \\ \dfrac{dS}{dt} = \dfrac{\Gamma G_0(N-N_0)S}{1+\varepsilon S} - \dfrac{S}{\tau_p} + \dfrac{\beta\Gamma N}{\tau_n} \end{cases} \tag{1}$$

where N is the carrier number, S is the photon number, I is the injected current, η_i is the injected efficiency, q is the electron charge, G_0 is the gain coefficient, N_0 is the carrier transparency number. Γ is the relative confinement factor, β is the spontaneous emission factor, τ_n is the carrier lifetime, τ_p is the photon lifetime, ε is the gain compression factor. The optical power P_O is proportional to the number of photons and has a scaling factor of k

$$P_O = kS \tag{2}$$

B. Rate equations with thermal behavior

P.V. Mena et al. represent the thermal behavior of VCSELs by introducing thermally relevant empirical offset current into the rate equations[13]. The offset current using a polynomial function of temperature

$$I_{off} = a_0 + a_1 T + a_2 T^2 + a_3 T^3 + a_4 T^4 + \cdots \tag{3}$$

After the addition of the offset current, the modified rate equations are

$$\begin{cases} \dfrac{dN}{dt} = \dfrac{\eta_i \left(I - I_{off}(T)\right)}{q} - \dfrac{N}{\tau_n} - \dfrac{G_0(N-N_0)S}{1+\varepsilon S} \\ \dfrac{dS}{dt} = \dfrac{\Gamma G_0(N-N_0)S}{1+\varepsilon S} - \dfrac{S}{\tau_p} + \dfrac{\beta\Gamma N}{\tau_n} \\ \dfrac{dT}{dt} = \dfrac{1}{\tau_{th}}(T_0 + (IV - P_O)R_{th} - T) \end{cases} \tag{4}$$

Temperature is described by the thermal rate equation, which takes into account the transient temperature increase due to heat dissipation. τ_{th} is the thermal time constant, T_0 is the ambient temperature, R_{th} is the VCSEL's thermal impedance (which expresses the relationship between the temperature variation of the VCSEL and the loss of power) and V is the voltage.

In order to obtain the LI curve for each ambient temperature, we also need the VI relationship. Assuming that the VI relationship of the laser does not change much at different operating temperatures, the VI relationship can be expressed as follows

$$V = IR_s + V_T ln\left(1 + \frac{I}{I_s}\right) \tag{5}$$

where R_s is the series resistance, V_T is the diode's thermal voltage, and I_S is the diode's saturation current.

C. Rate equations with noise behavior

To make the model more realistic, consider adding a noise term is needed. Spontaneous radiation is the cause of noise generation. We use the method of generating Langevin noise sources, which takes into account the interrelationship between carrier number noise sources and their phase noise sources[14].

$$\begin{cases} \dfrac{dN}{dt} = \dfrac{\eta_i\left(I - I_{off}(T)\right)}{q} - \dfrac{N}{\tau_n} - \dfrac{G_0(N-N_0)S}{1+\varepsilon S} + F_N(t) \\ \dfrac{dS}{dt} = \dfrac{\Gamma G_0(N-N_0)S}{1+\varepsilon S} - \dfrac{S}{\tau_p} + \dfrac{\beta\Gamma N}{\tau_n} + F_S(t) \\ \dfrac{d\phi}{dt} = \dfrac{1}{2}\alpha\left[\Gamma G_0(N-N_0) - \dfrac{1}{\tau_p}\right] + F_\theta(t) \end{cases} \tag{6}$$

Δt is the sampling interval. For the rate equations to be solved, we need to know the explicit forms for F_N, F_S and F_θ. They are constructed as follows

$$\begin{cases} F_S(t_i) = \sqrt{\dfrac{V_{SS}(t_i)}{\triangle t}}\, g_S \\ F_\theta(t_i) = \dfrac{1}{2[S(t_{i-1}+1)]}\sqrt{\dfrac{V_{SS}(t_i)}{\triangle t}}\, g_\theta \\ F_N(t_i) = \sqrt{\dfrac{V_{NN}(t_i) + 2k(t_i)V_{SN}(t_i)}{\triangle t}}\, g_N - k(t_i)F_S(t_i) - m(t_i)F_\theta(t_i) \end{cases} \tag{7}$$

where $V_{SS}(t_i)$, $V_{NN}(t_i)$, $V_{SN}(t_i)$, $k(t_i)$ and $m(t_i)$ are related to spontaneous radiation and expressed as

$$\begin{cases} V_{SS}(t_i) = \dfrac{2N(t_{i-1})}{\tau_n}\Gamma\beta[S(t_{i-1})+1] \\ V_{NN}(t_i) = \dfrac{2N(t_{i-1})}{\tau_n}[\Gamma\beta\tau_n S(t_{i-1})+1] \\ V_{SN}(t_i) = \dfrac{1}{\tau_p}[(N(t_{i-1})+N_0)S(t_{i-1}) + N(t_{i-1})] \\ k(t_i) = -\dfrac{V_{SN}}{V_{SS}} \\ m(t_i) = 2k(S(t_{i-1})+1) \end{cases} \tag{8}$$

We calculate each of the Gaussian random variables as one of the deviates

$$g_a = \begin{cases} \sqrt{-\log_{10} u_1}\, cos(2\pi u_2) \\ or \\ \sqrt{-\log_{10} u_1}\, sin(2\pi u_2) \end{cases}, a = S, Nor\theta \tag{9}$$

where u_1 and u_2 are uniformly distributed random number from -1 to 1.

D. Discrete–time domain model

Discretising the model in the time domain is actually about numerically predicting the change in carrier number N and photon number S at the next moment. To better describe the expression for the discretisation of the rate equations, we write the rate equations as functions of the current I, the carrier number N, the photon number S and the time t, denoted f and g as (10) respectively. We take the simple rate equations as an example, and the method is equally applicable when thermal behavior and noise are added.

$$\begin{cases} \dfrac{dN(t)}{dt} = f(I(t), N(t), S(t), t) = \dfrac{\eta_i I(t)}{q} - \dfrac{N(t)}{\tau_n} - \dfrac{G_0(N(t) - N_0)S(t)}{1 + \varepsilon S(t)} \\ \dfrac{dS(t)}{dt} = \mathrm{g}(N(t), S(t), t) = \dfrac{\Gamma G_0(N(t) - N_0)S(t)}{1 + \varepsilon S(t)} - \dfrac{S(t)}{\tau_p} + \dfrac{\beta\Gamma N(t)}{\tau_n} \end{cases} \tag{10}$$

We discretise the model in the time domain using the three methods (Euler's method, Midpoint method and Fourth order Runge-Kutta method) to obtain results for sampling the modulated signal at T_s [12].

a. Euler's method

Euler's method is one of the simplest numerical solutions. When this method is applied to the solution of the rate equation, the expressions for N and S at $t + T_s$ are given by (11) and the slope of change is obtained directly from the rate equations. However, this method has a large error and usually requires a high sampling rate to get better converged results.

$$\begin{cases} N(t + T_s) = N(t) + T_s \cdot f(I(t), N(t), S(t), t) \\ S(t + T_s) = S(t) + T_s \cdot f(N(t), S(t), t) \end{cases} \tag{11}$$

b. Midpoint method

The midpoint method is an improvement of Euler's method. Compared to the Euler's method, the midpoint method has a higher accuracy because the slope of the growing part is the slope at $t + T_s/2$. Such an approximation reduces the superposition of errors. We first compute carrier number N and photon number S and the slope at $t + T_s/2$.

$$\begin{cases} N\left(t + \dfrac{T_s}{2}\right) = N(t) + \dfrac{T_s}{2} \cdot f(I(t), N(t), S(t), t) \\ S\left(t + \dfrac{T_s}{2}\right) = S(t) + \dfrac{T_s}{2} \cdot g(N(t), S(t), t) \end{cases} \tag{12}$$

$$\begin{cases} N'\left(t + \dfrac{T_s}{2}\right) = f\left(I\left(t + \dfrac{T_s}{2}\right), N\left(t + \dfrac{T_s}{2}\right), S\left(t + \dfrac{T_s}{2}\right), t + \dfrac{T_s}{2}\right) \\ S'\left(t + \dfrac{T_s}{2}\right) = g\left(N\left(t + \dfrac{T_s}{2}\right), S\left(t + \dfrac{T_s}{2}\right), t + \dfrac{T_s}{2}\right) \end{cases} \tag{13}$$

Using the idea of Euler's method again, the expression at T_s can be expressed as

$$\begin{cases} N(t+T_s) = N(t) + T_s \cdot N'\left(t+\frac{T_s}{2}\right) = N(t) + T_s \cdot f\left(I(t), N\left(t+\frac{T_s}{2}\right), S\left(t+\frac{T_s}{2}\right), t+\frac{T_s}{2}\right) \\ S(t+T_s) = S(t) + T_s \cdot S'\left(t+\frac{T_s}{2}\right) = S(t) + T_s \cdot g\left(N\left(t+\frac{T_s}{2}\right), S\left(t+\frac{T_s}{2}\right), t+\frac{T_s}{2}\right) \end{cases} \quad (14)$$

c. Fourth order Runge-Kutta method

The fourth order Runge-Kutta method is a numerical method of fourth-order accuracy that typically produces more accurate results than lower-order methods such as the Euler's method or the midpoint method. The carrier number N and photon number S at $t + T_s$ can be expressed as

$$\begin{cases} N(t+T_s) = N(t) + \frac{T_s}{6} \cdot (k_1 + 2k_2 + 2k_3 + k_4) \\ S(t+T_s) = S(t) + \frac{T_s}{6} \cdot (m_1 + 2m_2 + 2m_3 + m_4) \end{cases} \quad (15)$$

where $k_i, m_i (i = 1,2,3,4)$ are expressed as

$$\begin{cases} k_1 = f(I(t), N(t), S(t), t) \\ m_1 = g(N(t), S(t), t) \end{cases} \quad (16)$$

$$\begin{cases} k_2 = f\left(I(t), N(t) + \frac{T_s}{2} \cdot k_1, S(t) + \frac{T_s}{2} \cdot m_1, t + \frac{T_s}{2}\right) \\ m_2 = g\left(N(t) + \frac{T_s}{2} \cdot k_1, S(t) + \frac{T_s}{2} \cdot m_1, t + \frac{T_s}{2}\right) \end{cases} \quad (17)$$

$$\begin{cases} k_3 = f\left(I(t), N(t) + \frac{T_s}{2} \cdot k_2, S(t) + \frac{T_s}{2} \cdot m_2, t + \frac{T_s}{2}\right) \\ m_3 = g\left(N(t) + \frac{T_s}{2} \cdot k_2, S(t) + \frac{T_s}{2} \cdot m_2, t + \frac{T_s}{2}\right) \end{cases} \quad (18)$$

$$\begin{cases} k_4 = f(I(t), N(t) + T_s \cdot k_3, S(t) + T_s \cdot m_3, t + T_s) \\ m_4 = g(N(t) + T_s \cdot k_3, S(t) + T_s \cdot m_3, t + T_s) \end{cases} \quad (19)$$

Ⅲ Simulation

A. Numerical simulation

We solve the rate equations in section II for the heat-containing behavior with three discrete methods. The model parameters are $\eta_i = 0.821$, $G_0 = 8.486 \times 10^5 s^{-1}$, $N_0 = 1.286 \times 10^6$, $\Gamma = 1$, $\beta = 2.68 \times 10^{-2}$, $\tau_n = 1.201\, ns$, $\tau_p = 2.884\, ps$, $\varepsilon = 3.888 \times 10^{-6}$, $R_{th} = 0.896℃/mW$, $a_0 = 2.213 \times 10^{-3}\, A$, $a_1 = -1.719 \times 10^{-4}\, A/K$, $a_2 = 3.355 \times 10^{-6} A/K^2$, $a_3 = 0\, A/K^3$, $a_4 = 0\, A/K^4$, $R_s = 149.8\Omega$, $V_T = 0.9366V$, and $I_s = 7.918 \times 10^{-5}\, A$. The modulation response curve of the device is discussed in [13], which also gives the possibility of direct modulation and equation solving for VCSEL. We modulate the laser at a constant current of 1mA with a modulation current of 4mA. The signal is a square wave signal with a bit rate of 2.4 Gbit/s. The optical output power graphs solved by the three methods respectively are as follows

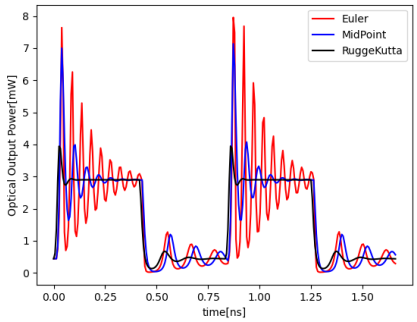

Fig. 1. Solution to the rate equations of three methods

From Fig. 1, it can be seen that the solution of the three methods have different degrees of oscillation, which is caused by the instability of numerical solution methods and the relaxation oscillation phenomenon of the laser. However, due to the fact that Euler and Midpoint methods may lead to instability easier in the numerical solution when solving problems with large oscillations or nonlinearities, thus creating a more severe oscillation in the results, these results are inaccurate. Increasing the sampling rate can solve such problems to a certain extent, but too high a sampling rate will increase the amount of computation, so the fourth order Runge-Kutta method, which gives better results with a lower sampling rate, becomes a better choice.

B. VCSEL characteristics

We discuss the model through the static LI characteristic and dynamic modulation characteristic of the VCSEL(Parameters for the simulation of the two characteristics are the same as the first device in part A).

We solve the system of differential equations through the steady state of each bias current, and the system of rate equations in Section II containing the thermal behavior is rewritten as (23), which are constraints on each other.

$$\begin{cases} \dfrac{dN}{dt} = 0 \\ \dfrac{dS}{dt} = 0 \\ \dfrac{dT}{dt} = 0 \end{cases} \tag{22}$$

The simulated result is shown in Fig. 2, which has a high degree of fit with the simulation results in [10] and show the output power flip at high currents.

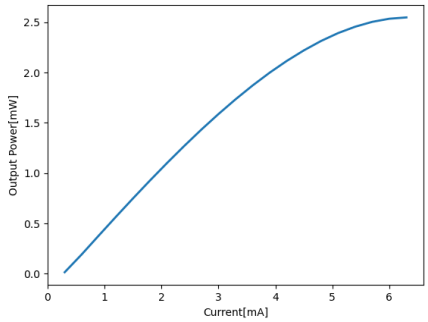

Fig. 2. LI curves for the device at 23°C

The modulation response $H(f)$ can be derived from small signal modulation of the VCSEL. Since parasitic capacitance is considered to be a key factor limiting the high-speed performance of this particular device. We consider the parasitic cut-off frequency in the expression for the frequency response, and normalized modulation response function can be expressed as[15]

$$|H(f)| = \frac{1}{\sqrt{\left[1+\left(\frac{f}{f_0}\right)^2\right]}} \frac{|Z|}{\sqrt{(2\pi fY)^2 + (-4f^2\pi^2 + Z)^2}} \tag{22}$$

Where f is the signal frequency, Y is the damping factor, Z is the resonance frequency factor respectively, and f_0 is the parasitic cut-off frequency and taken as 10 GHz. From Fig. 3Fig. 3, it can be seen that there is good agreement between the two sets of curves in [10], including the values of the resonance frequencies, the main difference being the amplitude of their resonance peak.

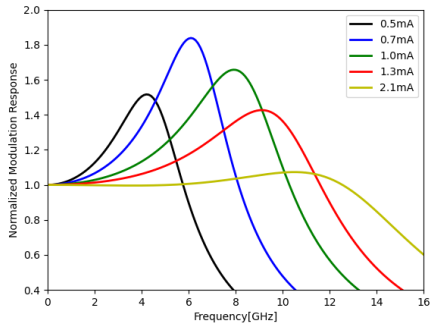

Fig. 3. Simulated modulation response curves for the device at 22°C

C. Compare with VPI and OptiSystem

In order to validate our model in the home-built simulation software, we compare our simulation results with those obtained by the mainstream simulation software VPI and OptiSystem. We modulate the input current for random NRZ coding and intercept some of the results for demonstration. The parameter settings of VCSEL are given by the simulation cases in the VPI software. The model parameters are $\eta_i = 1$, $G_0 = 1.613 \times 10^6 s^{-1}$, $N_0 = 2.232 \times 10^6$, $\Gamma = 0.03$, $\beta = 1 \times 10^{-4}$, $\tau_n = 2ns$, $\tau_p = 1.1526ps$, $\varepsilon = 2.6525 \times 10^{-5}$, $k = 1.0796 \times 10^{-6}$ and $\alpha = 3$.

Since there are some differences in the modelling of thermal behavior and parameter fitting between these software, we ignore the thermal behavior for the time being and focus on the simulation of noise. Then, we consider the simulation of adding noise. From Fig. 4 and Fig. 5, we can see that our simulation results from Python have a high degree of similarity with the two software, and both simulate stochastic dynamic processes.

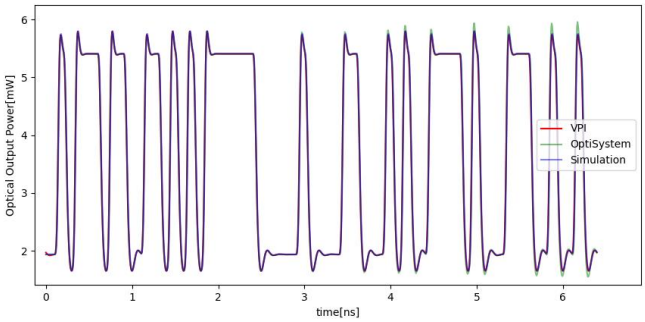

Fig. 4. Comparison of simulation results without noise

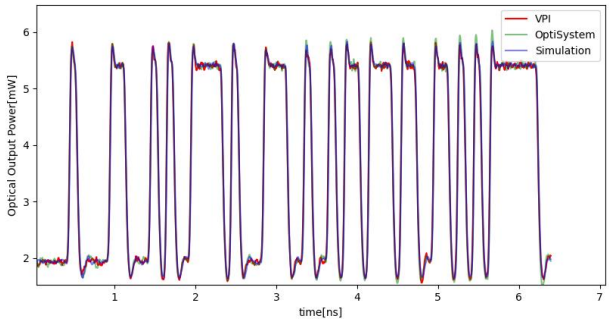

Fig. 5. Comparison of simulation results with noise

Ⅲ Conclusion

The rate equations for the interconversion of the number of carriers and the number of photons in a laser is described. The model considering thermal effects and noise describes the process more accurately, and the programming of the VCSEL model is facilitated by the time-domain discretisation, which lays a foundation for the study of the

characteristics of the VCSEL and the construction of the optical communication system in the simulation software. This paper discusses the rate equations for VCSEL and compares the simulation results with other literature and simulation software, and the results confirm the feasibility of the model.

References

[1] K. Iga, "Surface-emitting laser-its birth and generation of new optoelectronics field," IEEE Journal of selected topics in Quantum Electronics, vol. 6, no. 6, pp. 1201–1215

[2] K. Iga and H. Li, "Vertical-cavity surface-emitting laser devices," Cham, Switzerland: Springer, 2003

[3] F. Koyama, "Recent advances of vcsel photonics," Journal of Lightwave Technology, vol. 24, no. 12, pp. 4502–4513,

[4] M. Muller, W. Hofmann, G. Bohm, and M.-C. Amann, "Short-cavity long-wavelength vcsels with modulation bandwidths in excess of 15 ghz," IEEE Photonics Technology Letters, vol. 21, no. 21, pp. 1615–1617, 200

[5] M.-C. Amann and W. Hofmann, "Inp-based long-wavelength vcsels and vcsel arrays," IEEE Journal of Selected Topics in Quantum Electronics, vol. 15, no. 3, pp. 861–868

[6] J. S. Gustavsson, J. A. Vukusic, J. Bengtsson, and A. Larsson, "A comprehensive model for the modal dynamics of vertical-cavity surface-emitting lasers," IEEE journal of quantum electronics, vol. 38, no. 2, pp. 203–212, 20

[7] J. Gao, "High frequency modeling and parameter extraction for vertical-cavity surface emitting lasers," Journal of lightwave technology, vol. 30, no. 11, pp. 1757–1763,

[8] J. A. Tatum, D. Gazula, L. A. Graham, J. K. Guenter, R. H. Johnson, J. King, C. Kocot, G. D. Landry, I. Lyubomirsky, A. N. MacInnes et al. "Vcsel-based interconnects for current and future data centers," Journal of Lightwave Technology, vol. 33, no. 4, pp. 727–732

[9] N. Haghighi, P. Moser, and J. A. Lott, "Power, bandwidth, and efficiency of single vcsels and small vcsel arrays," IEEE Journal of Selected Topics in Quantum Electronics, vol. 25, no. 6, pp. 1–15,

[10] P. V. Mena, J. Morikuni, S.-M. Kang, A. Harton, and K. Wyatt, "A simple rate-equation-based thermal vcsel model," Journal of Lightwave Technology, vol. 17, no. 5, p. 865,

[11] J. C. Cartledge and R. Srinivasan, "Extraction of dfb laser rate equation parameters for system simulation purposes," Journal of Lightwave technology, vol. 15, no. 5, pp. 852–860

[12] K. Atkinson, W. Han, and D. E. Stewart, Numerical solution of ordinary differential equations. John Wiley & Sons, 2

[13] S. F. Yu, W. Wong, P. Shum, and E. H. Li, "Theoretical analysis of modulation response and second-order harmonic distortion in vertical-cavity surface-emitting lasers," IEEE journal of quantum electronics, vol. 32, no. 12, pp. 2139–2147

[14] M. Ahmed, M. Yamada, and M. Saito, "Numerical modeling of intensity and phase noise in semiconductor lasers," IEEE journal of quantum electronics, vol. 37, no. 12, pp. 1600–1610

[15] B. Thibeault, K. Bertilsson, E. Hegblom, E. Strzelecka, P. Floyd, R. Naone, and L. Coldren, "High-speed characteristics of low-optical loss oxide-apertured vertical-cavity lasers," IEEE Photonics Technology Letters, vol. 9, no. 1, pp. 11–13,